Anisotropy in the magnetic and transport properties of $Fe_{1-x}Co_xSb_2$

Rongwei Hu,[1,2] V. F. Mitrović,[2] and C. Petrovic[1]
[1]*Condensed Matter Physics and Materials Science Department, Brookhaven National Laboratory, Upton, New York 11973, USA*
[2]*Department of Physics, Brown University, Providence, Rhode Island 02912, USA*
(Received 2 June 2006; revised manuscript received 3 August 2006; published 30 November 2006)

Anisotropic magnetic and electronic transport measurements were carried out on large single crystals of $Fe_{1-x}Co_xSb_2$ ($0 \leqslant x \leqslant 1$). The semiconducting state of $FeSb_2$ evolves into metallic and weakly ferromagnetic by substitution of Fe with Co for $x < 0.5$. Further doping induces structural transformation from orthorhombic *Pnnm* structure of $FeSb_2$ to monoclinic $P21/c$ structure of $CoSb_2$, where semiconducting and diamagnetic ground state is restored again. Large magnetoresistance and anisotropy in electronic transport were observed.

DOI: 10.1103/PhysRevB.74.195130 PACS number(s): 71.28.+d, 71.30.+h, 75.20.Hr, 75.40.Cx

I. INTRODUCTION

Previous attempts to explain the unusual magnetic and electronic properties of the narrow-gap semiconductor FeSi[1,2] were based on either the itinerant magnetism model, the Kondo description, the mixed valence model, or the two-band Hubbard model, and started with Jaccarino's interpretation of an extreme narrowband-energy-gap model.[3–6] From this work, two different viewpoints have emerged. The first, proposed by Takahashi and Moriya,[3] treats FeSi as a nearly ferromagnetic semiconductor in an itinerant electron model. The second, as pointed out by Aeppli and Fisk,[4] takes FeSi as a transition metal version of the Kondo insulator with localized Fe moments. This viewpoint has the origin in the narrow-gap–high-density-of-states model that Jaccarino considered and then rejected. Experimental confirmation of that model was achieved by Mandrus *et al.*[7] and Park *et al.*[8] Other analogous $3d$ model systems are highly desired in order to study this problem, particularly those of noncubic and strongly anisotropic structures.

The magnetic properties of $FeSb_2$ strongly resemble those of FeSi.[9,10] Previous investigation of $FeSb_2$ has shown that the magnetism can be described by two effects: a thermally induced Pauli susceptibility and a low spin to high spin transition within the t_{2g} multiplet of Fe ion in octahedral crystal field.

In order to show the possible Kondo insulator to heavy-fermion metal transition, we perturbed the $FeSb_2$ electronic system by electron doping. We report the anisotropy in magnetic and electronic transport properties of $Fe_{1-x}Co_xSb_2$ as a function of Co content. The semiconducting ground state of $FeSb_2$ evolves into a metallic one by $x=0.1$. Further Co substitution induces weak ferromagnetism for $0.2 \leqslant x < 0.5$. Beyond $x=0.5$, there is a structural transformation from orthorhombic *Pnnm* to the monoclinic $P21/c$ structure of $CoSb_2$ and the restoration of the anisotropic semiconducting ground state for $0.5 \leqslant x < 1$. The weak ferromagnetism and high-temperature Curie-Weiss behavior is due to the small portion of localized Co ions. The large positive magnetoresistance arises in the $Fe_{1-x}Co_xSb_2$ electronic system, particularly for x values close to the metal-semiconductor crossover.

II. EXPERIMENTAL DETAILS

Single crystals were grown with the high-temperature flux method.[11,12] Their structure and composition were determined by analyzing powder x-ray diffraction (XRD) spectra taken with Cu Kα radiation ($\lambda = 1.5418$ Å) using a Rigaku Miniflex x-ray machine. The lattice parameters were obtained by fitting the XRD spectra using the Rietica software.[13] A JEOL JSM-6500 SEM microprobe was used for verifying the Co concentration. Crystals were oriented using a Laue camera and polished into rectangular bars along specific crystalline axes. Electrical contacts were made with Epotek H20E silver epoxy for a standard four-wire resistance measurement. The dimensions of the samples were measured by a high-precision optical microscope with 10 μm resolution. Magnetization, resistivity, and transverse magnetoresistance measurements were carried out in a Quantum Design MPMS-5 and a PPMS-9 varying the temperature from 1.8 to 350 K and applying a magnetic field up to 90 kOe. Polycrystalline averages were calculated from $M/H \equiv \chi = 1/3[\chi_a + \chi_b + \chi_c]$. Heat capacity data was collected in the PPMS-9 instrument using a relaxation technique.

III. RESULTS AND DISCUSSION

A. Crystal structure

Figure 1 shows the lattice constants and unit cell volume of $Fe_{1-x}Co_xSb_2$ as a function of nominal Co content, as determined by powder x-ray diffraction. As can be seen from Fig. 1, the end member structures of $Fe_{1-x}Co_xSb_2$ are orthorhombic *Pnnm* and monoclinic $P21/c$ for $FeSb_2$ and $CoSb_2$, respectively. Both $\hat{a}$ and $\hat{b}$ axes show a smooth linear decrease with increasing x for $0 \leqslant x < 0.5$. In contrast, the $\hat{c}$ axis expands with increasing x in the same doping range. At $x=0.5$, the $\hat{c}$ axis doubles in size and a monoclinic angle $\beta \neq 90°$ emerges, indicating a structural phase transition to lower symmetry of the unit cell.

In the monoclinic region, for $0.5 \leqslant x < 1$, the unit cell volume refers to that of a pseudomarcasite cell. This cell is related to the true unit cell of $CoSb_2$ (specified by $\vec{a}'$, $\vec{b}'$, $\vec{c}'$, and β') by vectorial equations of the following form: $\vec{a}' = (\vec{a} - \vec{c})/2$, $\vec{b}' = \vec{b}$, and $\vec{c}' = (\vec{a} + \vec{c})/2$.[14] In this doping regime as well, we observe a smooth evolution of a, b, and c lattice parameters with increasing x. The evolution is concurrent with a gradual increase of the monoclinic angle β', from 90.1° to 90.4° (Fig. 1, inset). This linear dependence on Co concentration, conforming to Vegard's law, demonstrates that

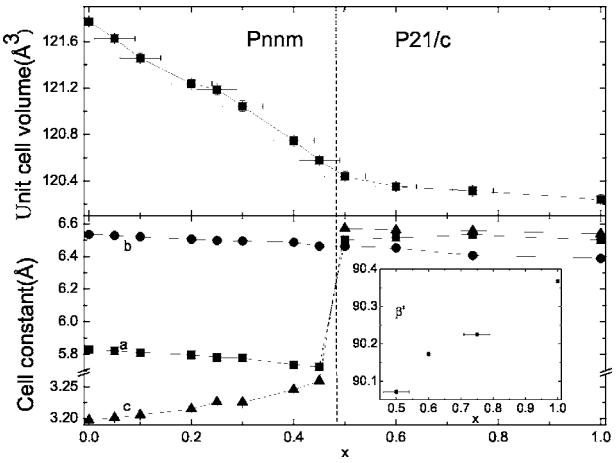

FIG. 1. Unit cell constants and volume of the series $Fe_{1-x}Co_xSb_2$ as a function of composition. Phase transition takes place at $x=0.5$. Dashed line represents the phase boundary between orthorhombic and monoclinic structures. Inset shows monoclinic angle β' in $P21/c$ structure.

Co successfully substitutes for Fe in the entire doping range. In addition, energy dispersive SEM for several nominal $x=0.25$ samples showed that the uncertainty in Co concentration among samples grown from different batches was $\Delta x=0.04$.

The anisotropy in the evolution of lattice parameters with Co content for $0 \leqslant x < 0.5$ is consistent with an increased occupancy of d_{xy} orbitals, directed toward nearest-neighbor Fe ions along $\hat{c}$ axis of the crystal.[10] Monoclinic distortion at $x=0.5$ increases the $\hat{c}$ axis and decreases the overlap of d_{xy} orbitals. The reduced overlap results in an enlargement of the gap within the t_{2g} multiplet[15] and causes a change in electronic transport properties. The electronic system gradually evolves toward a semiconducting ground state of $CoSb_2$ with the increase of Co concentration from $0.5 \leqslant x < 1$.

B. Magnetic properties

For $x=0$, the temperature dependence of the susceptibility is qualitatively the same for $H \| \hat{a}$, $\hat{b}$, and $\hat{c}$ as shown in Fig. 2(a). A diamagnetic to paramagnetic crossover at T in the vicinity of 100 K occurs when a field is applied parallel to the $\hat{c}$ axis. This crossover is absent when fields are applied parallel to the $\hat{a}$ and $\hat{b}$ axes. Furthermore, for $H \| \hat{a}$, $\hat{b}$ below 100 K, the susceptibility is temperature independent and can be described by a paramagnetic term $\chi_a = \chi_b = 2 \times 10^{-5}$ emu/mol. These observations contradict previous measurements of $FeSb_2$,[9] that reported a diamagnetic to paramagnetic crossover in the vicinity of 100 K for fields applied along all three axes. Our measurements were performed on large single-crystal samples, which eliminated the need for subtracting the background, which is often difficult to estimate with high certainty. Subtraction of the background was necessary in Ref. 9 due to very small mass of the $FeSb_2$ samples. Consequently, the intrinsic susceptibility of $FeSb_2$ determined on large single crystals, differs from Refs. 9 and 10 and is shown in Fig. 2(a).

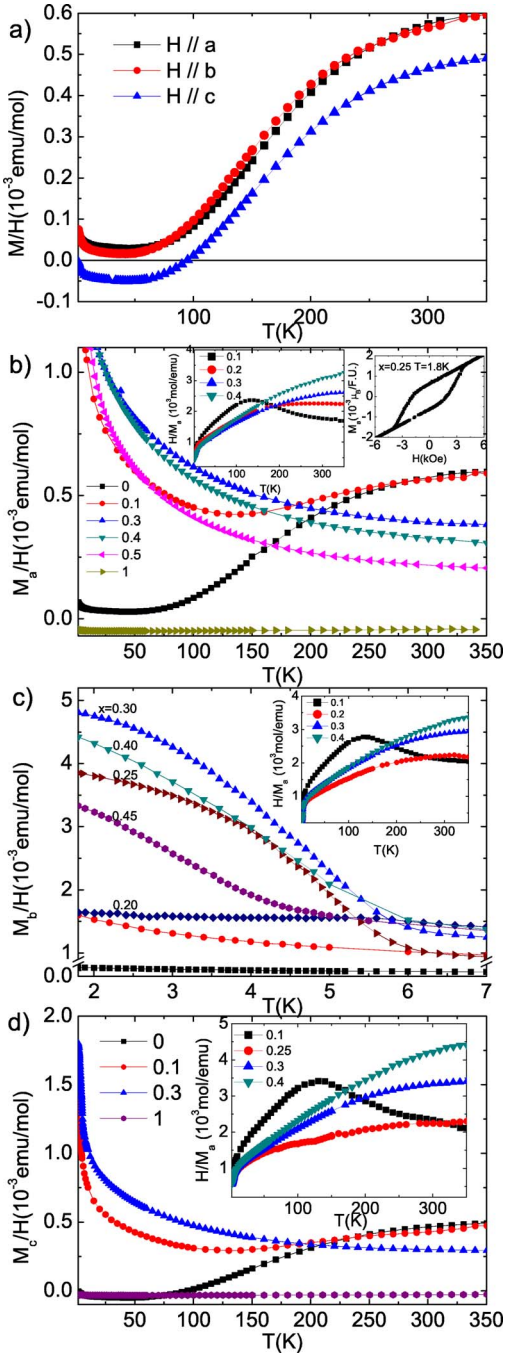

FIG. 2. (Color online) M/H vs T at $H=1000$ Oe along three crystalline axes. Some data of the series were omitted for clarity: (a) magnetization of $FeSb_2$ along all three axes. (b) Magnetization along $\hat{a}$ axis. Insets show the $1/\chi$ and also the hysteresis loop of $Fe_{0.75}Co_{0.25}Sb_2$. (c) Magnetization along $\hat{b}$ axis displays weak ferromagnetic transition at low temperatures for $0.2 \leqslant x \leqslant 0.45$. (d) $\hat{c}$ axis magnetization resembles those of $\hat{a}$ axis but shows no transitions at low temperatures.

In what follows, we explore to what extent different models can account for the observed paramagnetic moment and the temperature dependence of the susceptibility in $Fe_{1-x}Co_xSb_2$. In the free-ion model, the susceptibility χ is given by Jaccarino *et al.*[2] as

TABLE I. Parameters of the fits to the polycrystalline average of M/H data for $0 \leqslant x < 0.5$.

	$\chi(T)=\chi_{NB}+\chi_{CW}$								
x	Δ_χ (K)	W (K)	p	χ_0 (10^{-4} emu/mol)	μ_{eff} (μ_B)	Θ (K)	μ_{eff}/Co (μ_B)	T_c (K)	Ps (10^{-3} μ_B)
0	552	1.6	1.3	0.03	0	0			
	425	310	1.4	0.04					
0.05	531	235	2.1	0.3	0.41	−23			
0.10	511	471	2.5	1.6	0.79	−71			
0.20				4.5	0.14	110	0.70	6.6	1.49
0.25				3.3	0.24	104	0.99	6.0	1.73
0.30				3.0	0.32	77	1.08	6.8	1.87
0.40				1.5	0.54	17	1.35	7.3	1.19
0.45				1.5	0.54	16	1.20	6.4	0.75

$$\chi_{FI} = Ng^2\mu_B^2 \frac{J(J+1)}{3k_BT} \frac{2J+1}{2J+1+\exp(\Delta_\chi/k_BT)} + \chi_0.$$

This model describes thermal excitations from low to high spin states, separated by a spin gap Δ_χ. Moreover, in the simplest case, two spin states can be viewed as the $J=S=0$ spin singlet and the $S=1$ triplet state. Fitting the expression to the polycrystalline average of the magnetic susceptibility of $FeSb_2$ and setting $J=S$, we obtain $\chi_0=4.5\times10^{-6}$ emu/mol, $\Delta_\chi=527$ K, and $S=0.24$. The rather small value of S implies that the free-ion model may not be the explanation for the thermally induced paramagnetism at high temperatures, or that a small portion of Fe spins in the $S=0$ low spin d^4 ground state $(t_{2g},S=0)$ takes part in the spin-state transition.

The magnetic susceptibility of $FeSb_2$ can also be described by the narrowband–small-gap picture

$$\chi_{NB} = \frac{2N\mu_B^2 p \exp(\Delta_\chi/T)[\exp(W/T)-1]}{W[1+\exp(\Delta_\chi/T)]\{1+\exp[(\Delta_\chi+W)/T]\}} + \chi_0.$$

Here χ_{NB} is the Pauli susceptibility of an itinerant electron system with a density of states $N(E)$ consisting of two narrowbands of width W separated by a gap $E_g \equiv 2\Delta_\chi$, so that the chemical potential is defined as $\mu=W+\Delta_\chi$. The density of states is given by $N(E)=Np/W$, where N denotes the number of unit cells and p the number of states per unit cell. In this picture, χ_0 is the temperature-independent paramagnetic susceptibility. By fitting this model, we find the allowable values of parameters: $1.3<p<1.4$, $1.6\text{ K}<W<310$ K, $850\text{ K}<E_g<1100$ K. The result agrees with Ref. 9 but differs in a positive Pauli term, $\chi_0=3\times10^{-6}-4\times10^{-6}$ emu/mol, instead of a diamagnetic term.

At high temperatures for $0<x\leqslant0.45$, the magnetic susceptibility along all three crystalline axes can be described by two terms: a thermally induced paramagnetic moment with progressively smaller gap Δ_χ, and a growing Curie-Weiss term, due to Co substitution,

$$\chi(T) = \chi_{CW} + \chi_{NB},$$

where

$$\chi_{CW} = \frac{N\mu_{\text{eff}}^2}{3k_B(T-\Theta)}.$$

Results of fits for $0\leqslant x<0.5$ are shown in Table I. The gap Δ_χ decreases with increasing doping as x reaches 0.2. For $0.20\leqslant x\leqslant0.45$, the temperature dependence of the magnetic susceptibility above 180 K is characterized solely by the Curie-Weiss term and temperature-independent Pauli term χ_0.

The low-temperature magnetic properties of $Fe_{1-x}Co_xSb_2$ are anisotropic. For $H\|\hat{a}$ and $\hat{b}$, we observe a large increase of M/H values, a signature of ferromagnetic transition. Consequently, hysteresis loops, shown in the inset to Fig. 2(b), are observed for $0.2\leqslant x\leqslant0.45$ $(H\|\hat{b})$, as well as for $x=0.25$ $(H\|\hat{a})$ at $T=1.8$ K. The saturation moments P_s are listed in Table I. The Curie temperatures, determined by extrapolating the steepest slope of the M/H curve to $M=0$, vary from 5.9 to 7.2 K (Table I). This corresponds to the anomalies in the heat-capacity measurements (Fig. 6). $CoSb_2$ is diamagnetic in the whole experimental temperature range. As Fe is in the nonmagnetic $3d^4$ configuration, we assume that localized moment arises solely from the substituted Co atoms and, hence, Curie-Weiss term. To evaluate the high-temperature moment per Co atom, we fit the polycrystalline average of the magnetic susceptibility for temperatures ranging from 180 to 350 K with the Curie-Weiss law. We find the moment of μ/Co to be $1\pm0.35\mu_B$ for all the ferromagnetic x (Table I). This suggests the existence of polarized moments of Co^{2+} with low spin and quenched orbital momentum in the lattice. Therefore, we conclude that the weak ferromagnetism is due to the ordering of 0.2% of Co^{2+} moments. The fact that we were unable to detect any hysteresis loops above T_c and the absence of any sample dependence among sample within one batch of crystals, as well as among crystals from different batches, argues against extrinsic sources of weak ferromagnetism in $Fe_{1-x}Co_xSb_2$.

C. Electronic transport

Whereas the electronic transport of $FeSb_2$ is strongly anisotropic, there is much less dependence on "direction" for

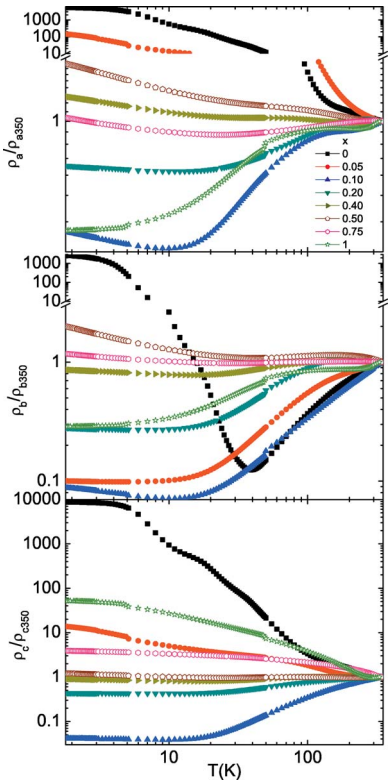

FIG. 3. (Color online) Normalized resistivity along all three axes as a function of temperature and different doping levels, x denoted by different shapes and colors. $Fe_{1-x}Co_xSb_2$ becomes metallic along all axes for $x>0.05$. With increasing x, the metallicity is lost in a crossover, where resistivity is nearly independent of temperature. Further increase of T leads to metallic behavior again along $\hat{a}$ and $\hat{b}$. However, resistivity along $\hat{c}$ axis evolves gradually from metallic to semiconducting. Below 40 K for $x=0$ and 0.05 samples the impurity tails up to 5 Ωcm are observed.

$Fe_{1-x}Co_xSb_2$. Figure 3 shows the normalized resistivity as a function of temperature along all three axes. Absolute values of the resistivity at $T=350$ K for samples with doping up to $x=0.4$ are listed in Table II. For $x=0$ ($FeSb_2$), there is metallic behavior above 40 K along the $\hat{b}$ axis, and activated behavior below that temperature. On the other hand, $FeSb_2$ is semiconducting for current applied along $\hat{a}$ and $\hat{c}$ axes. With a small amount of doping ($x=0.1$), the resistivity exhibits good metallic behavior over the whole temperature range,

TABLE II. Values of resistivity $Fe_{1-x}Co_xSb_2$ ($0\leqslant x\leqslant 0.4$) at 350 K.

x	ρ_a (mΩcm)	ρ_b (mΩcm)	ρ_c (mΩcm)
0	0.79	0.27	0.63
0.05	0.74	0.23	0.26
0.1	0.39	0.20	0.24
0.2	0.96	0.59	0.68
0.3	1.38	0.50	0.69
0.4	1.80	1.04	1.56

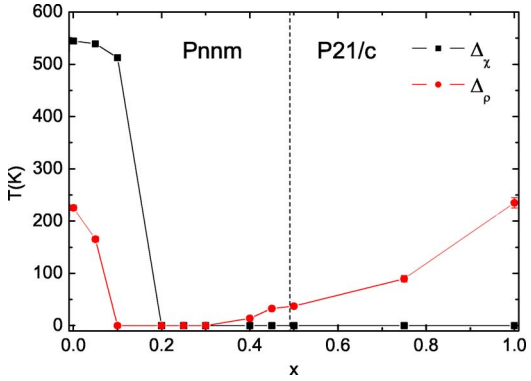

FIG. 4. (Color online) Spin and transport gaps as a function of Co concentration. The Curie-Weiss behavior is widely identified in the series. Both spin and transport gaps are shrinking due to Co impurity states, which likely reside in the gap.

and showing very small defect scattering ($\rho_0\sim 10$ μΩ cm) at 1.8 K, the lowest measured temperature.

For $0.1<x<0.4$, the electronic transport is metallic for current applied along all three principal crystalline axes. Metallicity induced by Co substitution is suppressed as the system evolves towards the region of the structural phase transition for $x\geqslant 0.5$, due to monoclinic distortion that causes doubling of the $\hat{c}$ axis and the consequent reduction of the overlap of d_{xy} orbitals. For $0.5\leqslant x\leqslant 1$ ($P21/c$ structure), a small anisotropy appears again, but it has different character comparing it to $0\leqslant x<0.5$ ($Pnnm$ structure). The structural change is likely one origin of that difference. More theoretical and experimental band structure work would be useful to shed light on the anisotropy of electronic transport of $Fe_{1-x}Co_xSb_2$ ($0.5\leqslant x\leqslant 1$).

For the semiconducting samples, we identify a regime of thermally activated resistivity above 40 K described by

$$\rho=\rho_0 e^{\Delta_\rho/2k_BT}.$$

Here, Δ_ρ is the transport energy gap. The activation energy for the transport gap is obtained at temperatures above 40 K. The spin gaps are obtained from the narrowband–small-gap model of the polycrystalline magnetic susceptibility. For $x=0.05$, the average value of Δ_ρ from $\rho_a(T)$ and $\rho_c(T)$ is shown (they agree within measurement error $\sim 10\%$), since ρ_b is metallic. For $0.5\leqslant x<1$ the value of Δ_ρ from ρ_c is shown since ρ_a and ρ_b are metallic. Near structural phase transition, the value of Δ_ρ from ρ_a is shown since ρ_b and ρ_c are metallic. A discrepancy between the spin and the transport gap values is evident (Fig. 4). A possible difference between the gaps in charge and spin excitation channels has also been observed in pure $FeSb_2$ (Ref. 9) as well as in FeSi.[16,17]

In $FeSb_2$, application of a magnetic field induces a large anisotropic positive magnetoresistance (Fig. 5) for current applied along the highly conductive $\hat{b}$ axis.[9] This effect is strongly enhanced in $Fe_{1-x}Co_xSb_2$, particularly for highly metallic samples. As an example, in Fig. 6 the effect in $Fe_{0.9}Co_{0.1}Sb_2$ is shown. In addition, magnetoresistance for pure $FeSb_2$ is plotted for comparison. Whereas magnetic

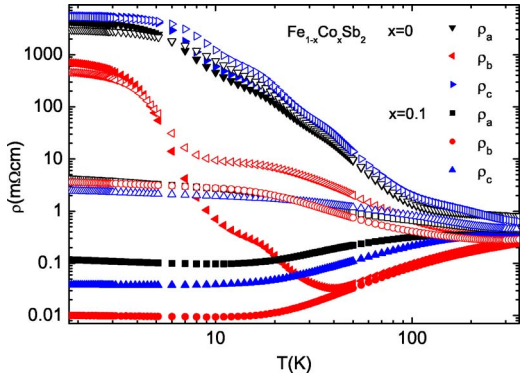

FIG. 5. (Color online) Large magnetoresistance for $x=0$ and moderately doped ($x=0.1$) highly metallic samples. Solid and open symbols denote data in 0 and 90 kOe applied fields, respectively.

field has little effect on the semiconducting electronic transport along the $\hat{a}$ and $\hat{c}$ axes in $FeSb_2$, for the $\hat{b}$ axis transport we observe up to two orders of magnitude of positive magnetoresistance at temperatures in the vicinity of the metal to semiconductor crossover temperature. Away from the crossover temperature the effect diminishes, below 5 K and in the vicinity of room temperature the application of a magnetic field has no effect on the $\hat{b}$ axis transport.

For $x=0.1$, this strong effect is more isotropic and is observed for current applied along all three crystalline axes. However for $I \| \hat{b}$, the effect is strongest. Below 10 K, the resistivity increases up to 2.5 orders of magnitude in an applied field of $H=90$ kOe. The transverse magnetoresistance (MR), defined as

$$\mathrm{MR} = \frac{[\rho(90\ \mathrm{kOe}) - \rho(0)]}{\rho(0)},$$

reaches 36 000% at $T=1.8$ K and ~30% at $T=300$ K in 90 kOe. This effect is comparable to the colossal magnetoresistance observed below room temperature in manganites. Furthermore, it is much higher at room temperature than in manganites. The origin of the magnetoresistance in $FeSb_2$ ($x=0$) is most likely due to the large mobility (μ) of carriers. The mobile carriers in a magnetic field move in cyclotron orbits specified by $\omega_c \tau \sim \mu H > 1$. Therefore, a strong positive magnetoresistance effect is expected in even a moderate field.[9]

Magnetic isotherms deviate from the quadratic relation for the ordinary metallic case, i.e., $\Delta\rho(H)/\rho_0 \propto H^2$, and there is a poor Kohler scaling for $Fe_{0.9}Co_{0.1}Sb_2$. The spin fluctuation mechanism proposed by Takahashi and Moriya[3] can be discarded based on the sign of the effect. Mainly because the spin fluctuation theory predicts negative magnetoresistance due to the thermally suppressed spin-fluctuation amplitude. In addition, the observed temperature dependence of magnetization does not contain $T^{3/2}$ and $T^{5/2}$ terms that arise from spin-wave and spin-wave–spin-wave interactions.

D. Heat capacity

The heat capacity C_p/T as a function of T^2 below 10 K is shown in Fig. 6. We observe a weak but clear signature of a

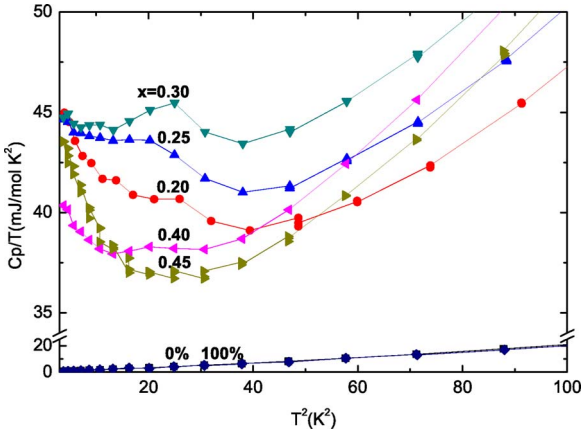

FIG. 6. (Color online) C_p/T as a function of T^2. Cusps correspond to ferromagnetic transition. Co doping gives rise to substantial increase in γ.

ferromagnetic transition in the vicinity of the T_C, as derived from magnetization measurements. By integrating C_p/T over T under this anomaly, the magnetic entropy contribution per Co is evaluated. For $x=0.3$, we find $\Delta S = 0.35\% k_B \ln 2$, in good agreement with the results obtained from the magnetization measurement. The end members of the $Fe_{1-x}Co_xSb_2$ series have negligible electronic specific heat $\gamma = 9.2 \times 10^{-3}$ mJ/mol K^2. This implies an negligible density of states at the Fermi level, i.e., an insulating state. The result agrees well with optical spectroscopy measurements that show a negligible Drude weight of $\sigma(\omega)$ at low frequencies.[18]

The changes in γ as a function of x are correlated with the evolution of the magnetic properties, since the saturation moment dependence for samples in the ferromagnetic region reaches a maximum value for $x=0.3$. Within the Kondo insulator framework, a metallic state with a large carrier mass enhancement is generated by a carrier induced closing of the hybridization gap. Consequently, the carrier mass enhancement leads to large γ value due to a renormalized band structure. The γ values observed in $Fe_{1-x}Co_xSb_2$ are comparable to those in the ferromagnetic regime of $FeSi_{1-x}Ge_x$ (Ref. 16) and $FeSi_{1-x}Al_x$, $Fe_{1-x}Co_xSi$ as well.[17,19] To estimate the carrier mass enhancement, we make the free-electron assumption. That is,

TABLE III. Sommerfeld coefficient and effective mass of carriers.

x	γ (mJ/molK^2)	m^* (m_e)
0.20	25.9	1.35
0.25	27.6	1.33
0.30	29.96	1.33
0.40	22.9	0.95
0.45	22.4	0.89

$$\gamma = \frac{\pi^2 k_B^2 N(E_F)}{3} = \frac{k_B^2 k_F m^*}{3\hbar^2}$$

with $k_F=(3\pi^2 n)^{1/3}$. The carrier density is denoted by n and is estimated to be equal to the Co concentration assuming one itinerant electron per Co^{2+}. This model implies only a small enhancement of carrier mass and disagrees with the Kondo insulator model (Table III). However, Hall constant measurements would be useful to determine the precise carrier density and, thus, provide a definitive test for the applicability of the Kondo insulator model. Furthermore, these measurements will help shed more light on the origin of the colossal magnetoresistance in this system.

IV. CONCLUSION

In summary, the $Fe_{1-x}Co_xSb_2$ electronic system exhibits two consecutive metal-to-semiconductor crossovers. The first is caused by electron doping of the semiconducting ground state of $FeSb_2$ for $x=0.1$. The second is induced by a structural change for doping levels in the vicinity of $x=0.5$. The density of states at the Fermi level increases due to the increased Co concentration, as shown in the rise of the electronic specific heat. The weak ferromagnetism induced by the polarization of a small portion of Co^{2+} ions arises in the metallic state for $0.2 \leqslant x < 0.5$. A colossal magnetoresistance as large as 36 000% is observed in the vicinity of the first metal to semiconductor crossover. The overall properties of $Fe_{1-x}Co_xSb_2$ can be understood in the narrowband–small-energy-gap framework, where Co substitution gives rise to impurity states in the gap, metallicity, and Curie-Weiss behavior. This is further supported by the recent LDA+U calculation of Lukoyanov *et al.* on $FeSb_2$, which indicates sharp peaks in the DOS at the edge of a small gap.[20] Possible consequence of the presence of magnetic Fe or an unknown ferromagnetic impurity would imply that the value of the direct Coulomb repulsion parameter U in Ref. 20 does not exceed the critical value of $U_C=2.6$ eV for all values of x in $Fe_{1-x}Co_xSb_2$ and that the weak ferromagnetism is extrinsic.[20]

ACKNOWLEDGMENTS

We thank Donavan Hall, T. M. Rice, P. C. Canfield, S. L. Bud'ko, Myron Strongin, and M. O. Dzero for useful communication and John Warren for SEM measurement. This work was carried out at the Brookhaven National Laboratory, which is operated for the U.S. Department of Energy by Brookhaven Science Associates (Grant No. DE-Ac02-98CH10886). This work was supported by the Office of Basic Energy Sciences of the U.S. Department of Energy.

[1] G. Föex, J. Phys. Radium **9**, 37 (1938).
[2] V. Jaccarino, G. K. Wertheim, J. H. Wernick, L. R. Walker, and S. Arajs, Phys. Rev. **160**, 476 (1967).
[3] Y. Takahashi and T. Moriya, J. Phys. Soc. Jpn. **46**, 1451 (1979).
[4] G. Aeppli and Z. Fisk, Comments Condens. Matter Phys. **16**, 155 (1992).
[5] C. M. Varma, Phys. Rev. B **50**, 9952 (1994).
[6] V. I. Anisimov, S. Y. Ezhov, I. S. Elfimov, I. V. Solovyev, and T. M. Rice, Phys. Rev. Lett. **76**, 1735 (1996).
[7] D. Mandrus, J. L. Sarrao, A. Migliori, J. D. Thompson, and Z. Fisk, Phys. Rev. B **51**, 4763 (1995).
[8] C.-H. Park, Z.-X. Shen, A. G. Loeser, D. S. Dessau, D. G. Mandrus, A. Migliori, J. Sarrao, and Z. Risk, Phys. Rev. B **52**, 16981 (1995).
[9] C. Petrovic, J. W. Kim, S. L. Bud'ko, A. I. Goldman, P. C. Canfield, W. Choe, and G. J. Miller, Phys. Rev. B **67**, 155205 (2003).
[10] C. Petrovic, Y. Lee, T. Vogt, N. Dj. Lazarov, S. L. Bud'ko, and P. C. Canfield, Phys. Rev. B **72**, 045103 (2005).
[11] P. C. Canfield and Z. Fisk, Philos. Mag. B **65**, 1117 (1992).
[12] Z. Fisk and J. P. Remeika, in *Handbook on the Physics and Chemistry of Rare Earths*, Vol. 12, edited by K. A. Gschneider and J. Eyring (Elsevier, Amsterdam, 1989).
[13] B. Hunter, in *International Union of Crystallography Commission on Powder Diffraction Newsletter*, No. 20 (Summer) http://www.rietica.org (1998).
[14] Einar Bjerkelund and Arne Kjekshus, Acta Chem. Scand. (1947-1973) **24**, 3317 (1970).
[15] J. B. Goodenough, J. Solid State Chem. **5**, 144 (1972).
[16] S. Yeo, S. Nakatsuji, A. D. Bianchi, P. Schlottmann, Z. Fisk, L. Balicas, P. A. Stampe, and R. J. Kennedy, Phys. Rev. Lett. **91**, 046401 (2003).
[17] J. F. DiTusa, K. Friemelt, E. Bucher, G. Aeppli, and A. P. Ramirez, Phys. Rev. B **58**, 10288 (1998).
[18] A. Perucchi, L. Degiorgi, R. Hu, C. Petrovic, and V. Mitrović, cond-mat/0510131 (unpublished).
[19] M. A. Chernikov, L. Degiorgi, E. Felder, S. Paschen, A. D. Bianchi, H. R. Ott, J. L. Sarrao, Z. Fisk, and D. Mandrus, Phys. Rev. B **56**, 1366 (1997).
[20] A. V. Lukoyanov, V. V. Mazurenko, V. I. Anisimov, M. Sigrist, and T. M. Rice, Eur. Phys. J. B **53**, 205 (2006).